Stabilization of the ferroelectric phase in lead zirconate ceramics doped with lithium niobate

H. T. Nguyen [a,*], S. V. Baryshnikov [b], A. Y. Milinskiy [b], E. V. Stukova [c], P. T. B. Thao [a]
[a] *Faculty of Electrical Engineering Technology, Industrial University of Ho Chi Minh City, 700000 Ho Chi Minh City, Vietnam*
[b] *Faculty of Physics and Mathematics, Blagoveshchensk State Pedagogical University, 675000 Blagoveshchensk, Russia*
[c] *Institute of Computer Science and Engineering, Amur State University, 675027 Blagoveshchensk, Russia*

The article presents results of a study on linear and nonlinear dielectric properties of lead zirconate-based ceramics synthesized from precursor powders of PbO and ZrO_2 with particle sizes of 500 nm and 20 nm, respectively. It was established that the addition of 5 mol% of lithium niobate induces a transformation from the antiferroelectric (AFE) to the ferroelectric state. Besides, the use of nanodispersed powders enables a reduction in sintering temperature compared to conventional technical ceramics.

(Received September 22, 2025; Accepted December 5, 2025)

Keywords: Lead zirconate, Ferroelectric phase, Solid-phase synthesis, Dielectric constant, Phase transitions

1. Introduction

Lead zirconate ($PbZrO_3$) was the first material identified as antiferroelectric (AFE) [1]. At temperatures above 230 °C, it exhibits a cubic crystal structure ($a \approx 4.15$ Å). Upon cooling to around 230 °C, a distinct dielectric anomaly is observed. In its low-temperature phase (T < 230 °C), PbZrO3 crystallizes in an orthorhombic structure with unit cell parameters of a = 5.888 Å, b = 11.758 Å, and c = 8.222 Å [2, 3]. It is generally accepted that a material can be classified as AFE if two key conditions are met: (i) an antipolar crystal arrangement, and (ii) the existence of a polar phase with comparable energy that can be induced by an external electric field [1]. The latter condition is especially crucial for functional applications of AFEs. The characteristic double hysteresis loops—strongly dependent on the applied electric field—result from an unstable transition between the AFE and ferroelectric (FE) phases. This field-induced phase transition allows AFE materials to be used in high-energy-density capacitors [4], large-displacement actuators [5], and electrocaloric devices [6, 7].

It was reported in [8, 9] that the FE phase of $PbZrO_3$ can emerge upon cooling below 230 °C and remain stable within a narrow intermediate temperature range of 10–25 °C even in the absence of external fields. Such an intermediate FE phase can also form in $PbZrO_3$ thin films. For instance, in lead zirconate films with a thickness of approximately 900 nm fabricated by sol–gel methods, the presence of an intermediate FE phase was observed, and its temperature stability could be extended under the application of an external electric field [10]. Theoretical

* Corresponding author: nguyenthuongfee@iuh.edu.vn
https://doi.org/10.15251/JOR.2025.216.789

studies [11] have established that epitaxial strain may influence the competition between AFE and FE phases. Calculations have also shown that surface effects contribute to the stabilization of the FE phase [12].

Controlling the stability of the FE state relative to the AFE state in thin films is considered a cornerstone for the future integration of such materials into electronic devices. A fundamental understanding of the mechanisms and conditions that promote the stabilization of the FE phase in $PbZrO_3$ is of critical importance. Study [13] demonstrated that, in FE composites, electrostatic interactions between constituents can enhance the stability of the FE state in one of the components. For example, the temperature range of the polar phase in potassium nitrate is extended in $(KNO_3)_{1-x}/(BaTiO_3)_x$ and $(KNO_3)_{1-x}/(LiNbO_3)_x$ composites. Similarly, the addition of barium titanate to lead zirconate ceramics significantly broadens the stability range of the FE phase in $PbZrO_3$ [14,15]. In the present work, we investigate the effect of $PbZrO_3$ doping on the formation of the polar phase in $PbZrO_3$ ceramics synthesized from nanodispersed PbO and ZrO_2 powders.

2. Materials and methods

Chemically pure PbO was used for the preparation of $PbZrO_3$ samples. The PbO powder was pre-milled for 1 hour using a MM 500 Control vibratory mill operating at a frequency of 30 Hz, resulting in an average particle size of approximately 500 nm. The second component was high-purity ZrO_2 (99.9%) with a particle size of 20 nm, supplied by Zhengzhou Haixu Abrasives Co., Ltd. (China).

As the additive for the preparation of composite ceramics, chemically pure lithium niobate ($LiNbO_3$) with an average particle size of 500 nm was used. Lithium niobate is a uniaxial FE material with a distorted perovskite structure; it exhibits a high Curie temperature (~ 1140 °C) and large spontaneous polarization (~ 70 μC/cm^2) [16, 17]. The $LiNbO_3$ additive was introduced at a concentration of 5 mol%. The PbO + ZrO_2 powder mixture was further mixed with $LiNbO_3$ and distilled water using a vibratory mill for 30 minutes. The resulting slurry was then dried and pressed into pellets without the use of plasticizers under a uniaxial pressure of 8×10^3 kg/cm^2. This pressure was selected to minimize lead loss during the sintering process. Our previous studies showed that, when pressed at 500 kg/cm^2 and sintered at 950 °C for 4 hours, the samples exhibited a mass loss of 7%–8%. In contrast, samples pressed at higher pressure and sintered under the same conditions showed a reduced mass loss of no more than 4%. The pressed specimens had a disk shape with a diameter of 10 mm and a thickness of 1.5 mm (Fig. 1). Note that the optimal temperature for the composite preparation was 1150 ℃, the estimation of which will be shown in this study.

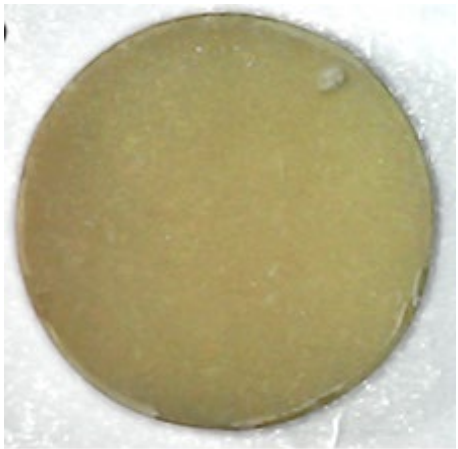

Fig. 1. Image of the composite samples prepared at 1150 ℃.

Morphology of the ceramic samples was examined using a Hitachi TM4000 Plus scanning electron microscope (Minato-ku, Tokyo, Japan). To determine the phase transition temperature of lead zirconate, differential thermal analysis (DTA) was performed by a Linseis STA PT 1600 thermal analyzer (Selb, Bayern, Germany). The dielectric properties were measured using an E7-25 LCR meter (Minsk, Belarus). All measurements were carried out in a "heating-cooling" mode with a temperature accuracy of 0.1 °C in a range from room temperature to 270 °C. To investigate the nonlinear dielectric response, nonlinear dielectric spectroscopy was employed [18]. During the experiment, the third-harmonic coefficient $\gamma_{3\omega}$, which is proportional to the spontaneous polarization, was measured as $\gamma_{3\omega} = I_{3\omega}/I_{\omega}$, where $I_{3\omega}$ is the amplitude of the third-harmonic signal and I_{ω} is the current at the fundamental frequency $\omega = 2\pi \cdot 2000\ s^{-1}$ [18, 19].

3. Experimental results.

The optimal temperature for preparation of the composite as stated above was estimated by measuring the maximum dielectric permittivity ε'_{max} at different sintering temperatures from 700 to 1200 °C (Fig. 2). According to our experimental data, the values of ε'_{max} increased in the first heating stage, then reached to maximum of 2400 at about 1150 °C and finally decreased with further heating. In this regard, the samples used for dielectric measurements in this study were synthesized at 1150 °C. As a result, the obtained composite had a granular structure with a grain size distributed in a range of approximately 200–100 nm as illustrated by scanning electron microscopy (SEM) image in Fig. 3.

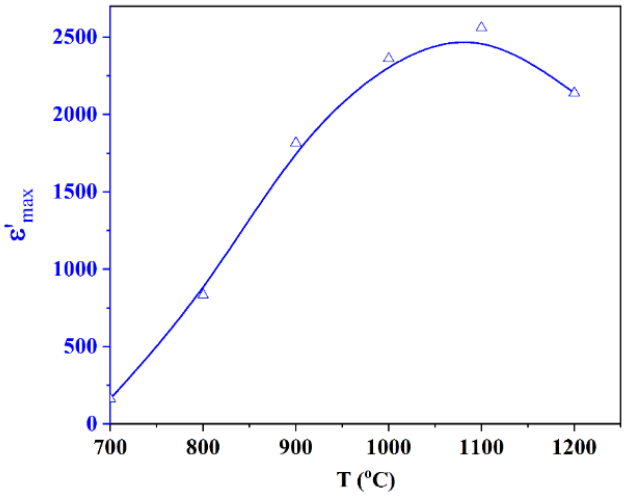

Fig. 2. Dependence of the maximum dielectric permittivity on sintering temperature for undoped samples.

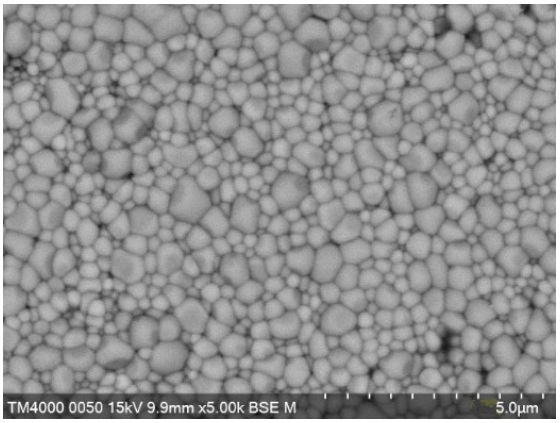

Fig. 3. SEM image of the surface of $PbZrO_3$ sample sintered at 1150 °C. SEM, scanning electron microscopy.

Fig. 4a shows the temperature dependences of $\varepsilon'(T)$ and $\gamma_{3\omega}(T)$ for $PbZrO_3$ ceramics sintered at 1150 °C without $LiNbO_3$. Upon cooling, a FE phase appears in the temperature range of 226–208 °C, as evidenced by the increase in the third-harmonic coefficient within this interval. The FE phase is bounded by two phase transitions, which are clearly observed in the DTA curve (Figure 4b). Above the phase transition, the Curie-Weiss law is obeyed with a Curie constant of $C = 0.83 \times 10^5$ °C and a Curie-Weiss temperature of $T_0 = 195$ °C. The dispersion of $\varepsilon'(\omega)$ in the frequency range from 1 kHz to 1 MHz does not exceed 5%. The temperature dependence of the dielectric loss tangent remains within the range of 0.01–0.02.

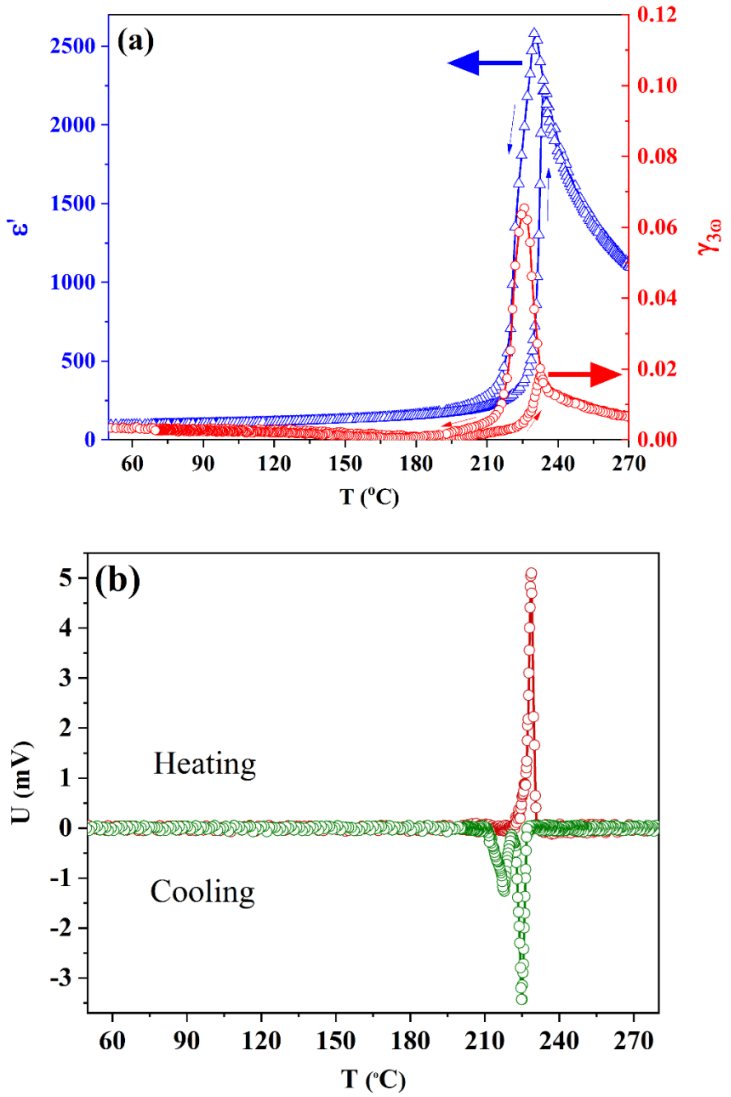

Fig. 4. Temperature dependences of ε'(T) and $\gamma_{3\omega}$(T) at 10 kHz (a) DTA curves (b) for undoped $PbZrO_3$ samples obtained at 1150 °C.

For $PbZrO_3$ ceramics with the addition of 5 mol% $LiNbO_3$ (Figure 5a), a decrease in the phase transition temperature to 202 °C is observed, along with an increase in dielectric permittivity and the presence of a FE phase during both heating and cooling. This is evidenced by the rise in the third-harmonic coefficient near the phase transition. The DTA curve shows one phase transition upon heating and one upon cooling (Figure 5b). In addition, the DTA curves indicate a broadening of the phase transition region compared to pure $PbZrO_3$. For these samples, the Curie-Weiss law is satisfied above the transition temperature, with a Curie constant of $C = 0.8 \times 10^5$ °C and a Curie-Weiss temperature of T_0 = 180 °C. The dispersion of $\varepsilon'(\omega)$ in the frequency range from 1 kHz to 1 MHz does not exceed 5%. The temperature dependence of the dielectric loss tangent is of the same order of magnitude as that observed in undoped $PbZrO_3$ samples. The presence of an FE state is also confirmed by the observation of polarization hysteresis loops in the temperature range from 40 °C up to the phase transition temperature (Fig. 6). During the experiment, the maximum applied electric field did not exceed 10 kV/cm. Under these conditions, full polarization saturation was not achieved, and therefore, the actual values of spontaneous polarization may be higher than those shown in this graph.

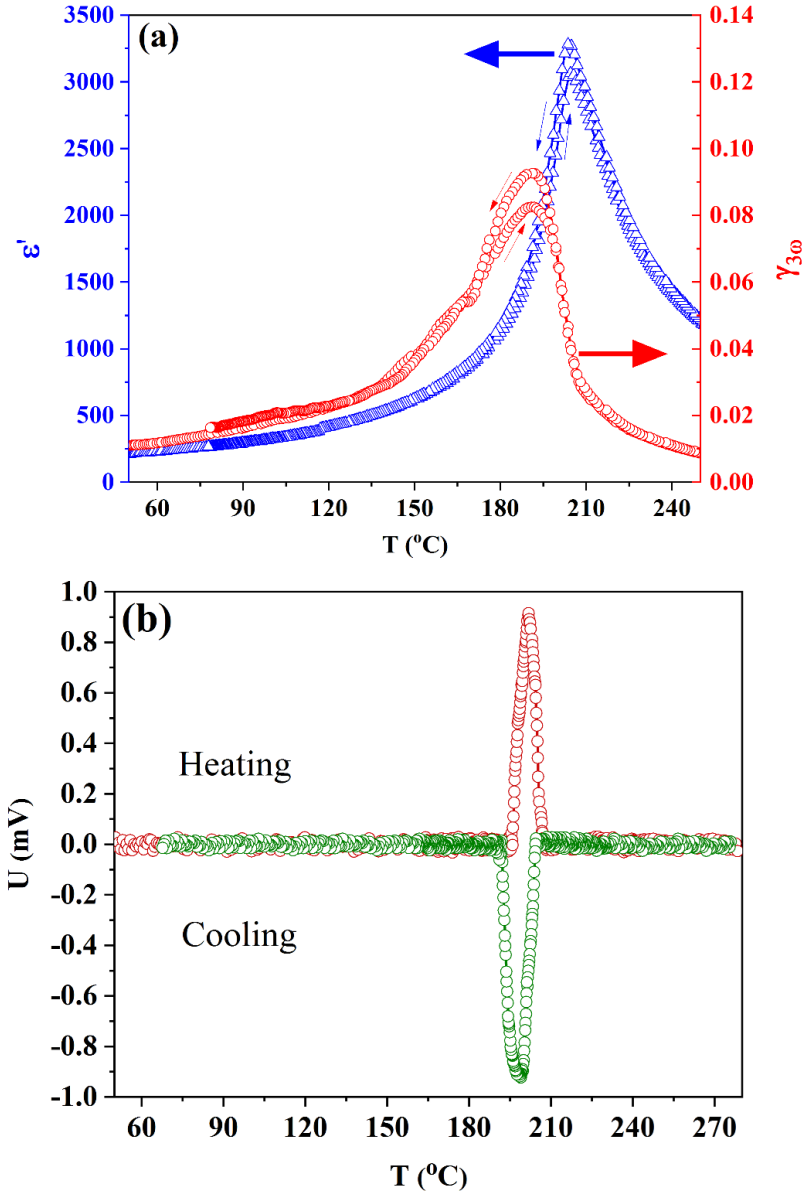

Fig. 5. Temperature dependences of ε'(T) and $\gamma_{3\omega}$(T) at 10 kHz (a), and DTA curves (b) for 5 mol% $LiNbO_3$-doped $PbZrO_3$ samples obtained at 1150 °C.

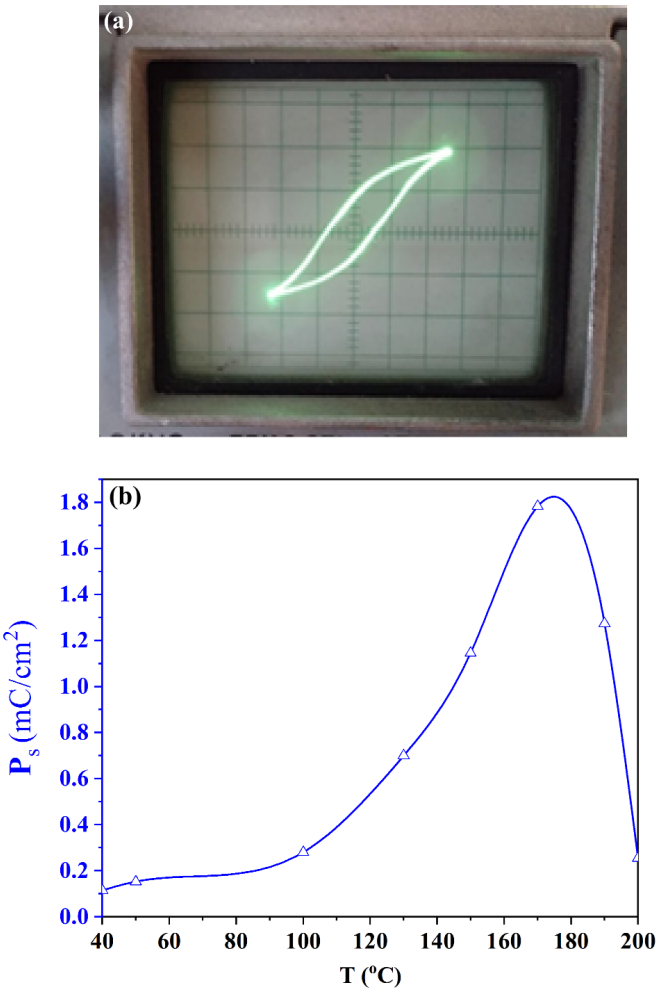

Fig. 6. P-E hysteresis loop (a) and the corresponding exported saturation polarization Ps at different temperatures (b) for samples of $PbZrO_3$ with 5 mol% $LiNbO_3$.

Based on the above description for the undoped $PbZrO_3$ ceramics, the FE phase appears only during cooling and is confined between two phase transitions. In contrast, in $PbZrO_3$ ceramics doped with 5 mol% $LiNbO_3$, the FE phase is limited only from above by the phase transition temperature at 202 °C, while upon cooling, the spontaneous polarization decreases gradually over a broad temperature range. Due to the differences in ionic radii and valence states between Li and Pb, as well as Nb and Zr, the formation of a solid solution between $PbZrO_3$ and $LiNbO_3$ is unlikely. Therefore, the lead zirconate ceramics with lithium niobate addition should be considered as a composite material.

4. Theoretical Models and Discussions

The stability of the AFE or FE phase in $PbZrO_3$ has been discussed in several publications [12, 20–22], which suggest that the stabilization of the FE phase in $PbZrO_3$ may occur due to mechanical stresses or applied electric fields. When comparing the thermal expansion coefficients of $PbZrO_3$ ($28 \times 10^{-6}\ K^{-1}$ [16]) and $LiNbO_3$ ($\sim 25 \times 10^{-6}\ K^{-1}$ [17]), the difference is minimal and unlikely to induce significant internal stresses.

The magnitude of local electric fields arising in the $PbZrO_3$-$LiNbO_3$ system depends on temperature and the concentration of $LiNbO_3$ particles. To estimate the maximum electric fields in ceramics containing $LiNbO_3$ particles, let us consider a monodomain $LiNbO_3$ particle in the shape of a cube with an edge length of 500 nm. The dipole moment of such a particle is given by $d = P_s.v$, which in SI units yields $d = 8.75 \times 10^{-20}$ $C \cdot m$. The electric field strength generated by such a particle in the surrounding medium at a distance R from the particle is defined as

$$E = \frac{1}{4\pi\varepsilon\varepsilon_o}\frac{d\cos\vartheta}{R^3} \quad (1)$$

where ε and ε_o are the dielectric permittivity of the medium and vacuum, respectively, and θ is the angle between the dipole axis and the direction toward the point at which the electric field is calculated. Obviously, the maximum electric field strength in the direction of P_s, for a medium with a dielectric constant ε ranging from 10^3 to 10^2, at a distance of one micron, lies within the range of $E \approx 1.57 \times 10^4$ V/cm to $E \approx 1.57 \times 10^5$ V/cm. Such field strengths are sufficient to induce the FE state in lead zirconate. A similar phenomenon has been observed in the composites $(DIPAB)_{1-x}/(PbTiO_3)_x$ and $(DIPAC)_{1-x}/(PbTiO_3)_x$, where the sequence of phase transitions of diisopropylammonium bromide and chloride is altered [23, 24].

5. Conclusions

In summary, the effect of introducing 5 mol% lithium niobate ($LiNbO_3$) into lead zirconate ($PbZrO_3$) ceramics synthesized from nanodispersed powders on the phase transitions and dielectric properties showed that the addition of $LiNbO_3$ reduced the FE-high-temperature phase transition point by about 18 °C from ~220 °C for pure $PbZrO_3$ to ~202 °C for the composite ceramic. In pure $PbZrO_3$, the FE phase appeared only upon cooling and was confined to a narrow temperature interval, whereas in the composite ceramic the FE phase occurred upon both heating and cooling, limited only by the upper boundary at ~202 °C, with spontaneous polarization gradually decreasing in the cooling process. Stabilization of the FE phase can be explained by electric interactions between $PbZrO_3$ and $LiNbO_3$ particles. Indeed, the conducted calculations indicated that a monodomain $LiNbO_3$ particle with a size of 500 nm might create local electric fields on the order of 10^4–10^5 V/cm at a distance of 1 μm in the $PbZrO_3$ dielectric matrix, which induced a FE state in the surrounding matrix. Microstructural analysis by scanning electron microscopy revealed an average grain size of about 500 nm under optimal sintering conditions (1100–1150 °C), contributing to high density and homogeneity of the material. The study of the nonlinear dielectric response through the third harmonic coefficient confirmed the presence of a FE phase and was consistent with the DTA data. The obtained results demonstrated the possibility of targeted stabilization of the FE phase in $PbZrO_3$ by introducing FE $LiNbO_3$ inclusions, thereby expanding the operating temperature range and improving the dielectric properties of the material.

Availability of Data and Materials

The datasets used and analyzed during the current study are available from the corresponding author on reasonable request.

Author Contributions

HTN analyzed the experimental data and prepared manuscript. SVB contributed to using the theoretical model for explaining data. AYM and PTBT conducted experiments. All authors read and approved the final manuscript.

Acknowledgment

We would like to express our gratitude to all those who helped us during the writing of this manuscript. Thanks to all the peer reviewers for their opinions and suggestions.

Funding

This research received no external funding.

Conflict of Interest

The authors declare no conflict of interest

References

[1] E. Sawaguchi, H. Maniwa, S. Hoshino, Physical Review Journals Archive **83**(5), 1078(1951). https://doi.org/10.1103/PhysRev.83.1078

[2] G. Shirane, E. Sawaguchi, Y. Takagi, Physical Review Journals Archive **84**(3), 476(1951). https://doi.org/10.1103/PhysRev.84.476

[3] B. Jaffe, W. R. Cook, H. Jaffe, Piezoelectric Ceramics, Academic Press (London, New York), 317 p. (1971). https://doi.org/10.1016/0022-460X(72)90684-0

[4] H. J. Lee, S. S. Won, K. H. Cho, J. H. Lee, K. C. Lee, Applied Physics Letters **112**(9), 092901(2018). https://doi.org/10.1063/1.5018659

[5] S.-T. Zhang, A. B. Kounga, W. Jo, C. Jamin, K. Seifert, T. Granzow, J. Rödel, Advanced Materials **21**(46), 4716(2009). https://doi.org/10.1002/adma.200901516

[6] Y. Liu, J. F. Scott, B. Dkhil, Applied Physics Reviews **3**(3), 031102(2016). https://doi.org/10.1063/1.4960787

[7] J. Parui, S. B. Krupanidhi, physica status solidi (RRL) – Rapid Research Letters **2**(5), 230(2008). https://doi.org/10.1002/pssr.200802142

[8] V. J. Tennery, Journal of the American Ceramic Society **49**(9), 483(1966). https://doi.org/10.1111/j.1151-2916.1966.tb13304.x

[9] B. A. Scott, G. Burns, Journal of the American Ceramic Society **55**(6), 331(1972). https://doi.org/10.1111/j.1151-2916.1972.tb11296.x

[10] J. Zhai, H. Chen, Applied Physics Letters **82**(16), 2673(2003). https://doi.org/10.1063/1.1569042

[11] L. Pintilie, K. Boldyreva, M. Alexe, D. Hesse, Journal of Applied Physics **103**(2), 024101(2008). https://doi.org/10.1063/1.2829816

[12] S. E. Reyes-Lillo, K. M. Rabe, Physical Review B **88**(18), 180102(2013). https://doi.org/10.1103/PhysRevB.88.180102

[13] E. V. Stukova, S. V. Baryshnikov, Inorganic Materials: Applied Research **2**(5), 434(2011). https://doi.org/10.1134/S2075113311050288

[14] W. Chaisan, S. Ananta, T. Tunkasiri, Current Applied Physics **4**(2), 182(2004). https://doi.org/10.1016/j.cap.2003.11.008

[15] G. Shirane, Physical Review **86**(2), 219(1952). https://doi.org/10.1103/PhysRev.86.219

[16] M. E. Lines, A. M. Glass, Principles and Applications of Ferroelectrics and Related Materials, Clarendon Press (Oxford), 694 p. (2001).https://www.amazon.co.uk/Principles-Applications-Ferroelectrics-Materials-Physical/dp/019850778X

[17] A. M. Prokhorov, Yu. S. Kuz'minov, Physics and Technology of Ferroelectric Crystals for Laser Radiation Control Devices, Nauka (Moscow)/CRC Press, 468 p. (1990).https://www.amazon.co.uk/Ferroelectric-Crystals-Radiation-Control-Optoelectronics/dp/0750300477

[18] S. Miga, J. Dec, W. Kleemann, Review of Scientific Instruments **78**(3), 033902(2007). https://doi.org/10.1063/1.2712792
[19] S. V. Baryshnikov, A. Yu. Milinskiy, E. V. Stukova, Glass and Ceramics **81**(3), 152(2024). https://doi.org/10.1007/s10717-024-00662-5
[20] K. Roleder, J. Dec, Journal of Physics: Condensed Matter **1**(9), 1503(1989). https://doi.org/10.1088/0953-8984/1/9/001
[21] S. Lisenkov, Y. Yao, N. Bassiri-Gharb, I. Ponomareva, Physical Review B **102**(10), 104101(2020). https://doi.org/10.1103/PhysRevB.102.104101
[22] Z. Yu, N. Fan, Z. Fu, B. He, S. Yan, H. Cai, X. Chen, L. Zhang, Y. Zhang, B. Xu, G. Wang, F. Xu, Nature Communications **15**, 3438(2024). https://doi.org/10.1038/s41467-024-47715-5
[23] S. V. Baryshnikov, E. V. Stukova, T. A. Meredelina, St. Petersburg State Polytechnical University Journal. Physics and Mathematics **12**(3), 17(2019). https://doi.org/10.18721/JPM.12302
[24] E. V. Stukova, S. V. Baryshnikov, St. Petersburg State Polytechnical University Journal. Physics and Mathematics **13**(2), 12(2020). https://doi.org/10.18721/JPM.13202